Computers and Geotechnics 162 (2023) 105604

Contents lists available at ScienceDirect

Computers and Geotechnics

journal homepage: www.elsevier.com/locate/compgeo

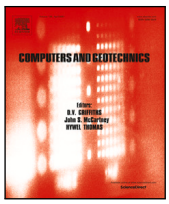

Research paper

Finite element-based probabilistic framework including Bayesian inference for predicting displacements due to tunnel excavation

Jocelyn Minini [a,*], Yi Zhang [b], Marc Groslambert [c], Stéphane Commend [a,c,*]

[a] School of Engineering and Architecture, HES-SO, University of Applied Sciences Western Switzerland, 1700 Fribourg, Switzerland
[b] Technical department, Eiffage Génie Civil, 78140 Vélizy-Villacoublay, France
[c] GeoMod SA, 1000 Lausanne, Switzerland

ARTICLE INFO

Keywords:
Probabilistic analysis
Bayesian inference
Metamodelling
Serviceability limit state
Reliability
Non-linear finite element modelling

ABSTRACT

Excessive settlements due to tunnel excavation in urban sites may affect the stability of sensitive buildings, and additional design costs are needed to prevent these effects. In this article, a finite element-based probabilistic framework is presented and applied to a real-world case study to estimate tunnel-induced settlements. This probabilistic analysis framework consists of the following four fundamental elements: a sensitivity analysis to identify key parameters, an a priori reliability analysis using metamodels to calculate reliability indices and probabilities of failure, field monitoring results (e.g., settlements) and a Bayesian inverse analysis using the field measurements to update the probabilities of failure a posteriori. This framework is materialized through the linking of ZSOIL, a non-linear finite element soil–structure interaction software, and UQLab, a MATLAB®-based uncertainty quantification toolbox. With the application of this framework to a real-world case study in the Grand Paris Express project, key geotechnical parameters can be identified, reliability indices and probabilities of failure can be computed using metamodelling-powered Monte Carlo (MCS) and adaptive kriging Monte Carlo simulations (AKMCS). Finally, using Bayesian inverse analyses to update prior knowledge and refine posterior prediction, the probability that the settlements exceed acceptable values can be reduced, potentially leading to design cost savings.

1. Introduction

The need to construct tunnels, especially in urban environments, is increasing due to the densification of the population. Tunnel construction inevitably induces ground settlement due to stress relief during excavation. These movements, particularly settlements, may significantly affect existing buildings and utilities, as well as to structures under construction in the vicinity of the tunnel (Leca and New, 2007; Zhang and Hamet, 2022). Regarding urban projects, limiting tunnel-induced displacements is an important problem. These displacements should remain within an acceptable level for the chosen design, which can be calculated using either analytical solutions or numerical simulations. Among them, the finite element method (FEM) is commonly used for soil–structure interaction analyses to obtain precise and complete results with carefully defined calculation hypotheses and characteristic values of geotechnical parameters (CEN, 2004; Lees, 2016). However, uncertainties in model parameters and associated model response variations are difficult to treat by deterministic or even semi-probabilistic methods. Therefore, probabilistic methods may be suitable for considering these uncertainties (Duncan, 2000; Baecher and Christian, 2003; Zhang and Ng, 2005; Lacasse and Nadim, 2007; Phoon and Ching, 2018). Thus, by applying probabilistic methods (Hsiao et al., 2008; Zhang and Goh, 2012; Xiao et al., 2016; Zevgolis et al., 2018; Al-Bittar et al., 2018; Chen et al., 2019; Li et al., 2021), geotechnical problems can be statistically analysed. Moreover, in recent decades, reliability-based analyses (Fellin et al., 2005; Ang and Tang, 2007; Lemaire, 2009; Marelli and Sudret, 2014; Fenton et al., 2016; Low, 2017; Melchers and Beck, 2018) have become increasingly practised due to the emergence of computational methods.

An annex concerning the reliability of geotechnical structures has been added to ISO 2394-2015 (Phoon and Retief, 2015). In the JCSS probabilistic model (JCSS, 2001) and Eurocodes (CEN, 2002), reliability is expressed in terms of reliability indices or probabilities of failure and used to measure the structural safety, maintainability, durability and robustness. For example, in the Eurocodes, three reliability classes RC1, RC2 and RC3 are defined. If the ultimate limit state (ULS) target reliability index is well defined (CEN, 2002; Zhang and Toutlemonde, 2022), the serviceability limit state (SLS) target reliability index is not explicitly expressed (CEN, 2002; Zhang and Commend, 2021).

* Correspondence to: Institute of Construction and Environmental Technologies, School of Engineering and Architecture, 1700 Fribourg, Switzerland.
E-mail addresses: jocelyn.minini@hefr.ch (J. Minini), stephane.commend@hefr.ch (S. Commend).

https://doi.org/10.1016/j.compgeo.2023.105604
Received 9 January 2023; Received in revised form 7 May 2023; Accepted 15 June 2023
Available online 6 July 2023

Nomenclature

Abbreviations

AKMCS	Adaptive Kriging Monte Carlo Simulation
CI	Confidence interval
ED	Experimental design
LOO	Leave-one-out cross validation
MCS	Monte Carlo Simulation
MCMC	Markov Chain Monte Carlo
PCK	Polynomial Chaos Kriging
PDF	Probability Density Function
SLS	Serviceability limit state

Calligraphic

$\mathcal{A}$	Multi-set indices
$\mathcal{D}$	Domains
$\mathcal{G}$	Gumbel distribution
$\mathcal{L}$	Likelihood function
$\mathcal{LN}$	Lognormal distribution
$\mathcal{M}$	FE model
$\widehat{\mathcal{M}}$	Metamodel
$\mathcal{N}$	Normal distribution
$\mathcal{X}$	Experimental design (FE Input)
$\mathcal{Y}$	Experimental design (FE Response)
$\mathcal{Z}$	Measurements set

Greek

β_i	Beta reliability index
ϵ	Discrepancy term
λ	Confinement loss
μ_X	Expectation (moment)
φ	Friction angle
σ	Stress
σ_X	Standard deviation (moment)
Ψ_α	Polynomial basis
ψ	Dilatation angle
ν_{ur}	Unloading–reloading Poisson's ratio

Latin

c	Cohesion
c_u	Undrained cohesion
D	Total variance
D_i	Partial variances
f_X	PDF
Err_{LOO}	Leave-one-out empirical error
err_{LOO}	Leave-one-out relative empirical error
E_{oed}	Tangent oedometric modulus
E_{50}	Secant modulus ($\frac{1}{2}$ of deviatoric stress failure)
E_{ur}	Unloading–reloading modulus
m	Stiffness exponent (minor stress formulation)
Mo	Mode of a statistical distribution
P_f	Probability of failure
S_i^T	Total Sobol' indices
T_{FE}	Time needed by the FE software to generate the ED
$U_y(x)$	Settlement at position x
y_α	Polynomial coefficients

According to the literature, the target SLS reliability index beta is $\beta_i = 1.5$, corresponding to $P_f = 6.7\%$ over a period of 50 years (Gulvanessian et al., 2012). Therefore, more work on SLS reliability assessment is needed.

Although probabilistic methods have been commonly applied to geotechnics, it can be found from the above literature that the majority of previous studies have focused either on random variables (Zhang and Goh, 2012; Xiao et al., 2016) or analytical solutions (Hsiao et al., 2008; Zevgolis et al., 2018; Chen et al., 2019; Li et al., 2021). Few probabilistic computations, including uncertainty quantification, sensitivity, reliability and Bayesian analyses, have been carried out with finite element models. Therefore, the aim of this paper is to present a probabilistic analysis framework based on metamodelling-powered finite element calculations.

The structure of this paper is organized as follows. First, a probabilistic analysis framework using finite element modelling is proposed, consisting of four fundamental elements: a sensitivity analysis with Sobol and Kucherenko methods to identify key geotechnical parameters, a reliability analysis to compute probabilities of failure, field monitoring observations, and a Bayesian inverse analysis using field measurements to improve the prediction performance. Then, a real-world case study regarding tunnel excavation in the White House Station of the Grand Paris Express project is carried out to demonstrate the power of this probabilistic analysis framework. Finally, concluding remarks are provided.

2. Probabilistic framework & governing equations - A toolbox

A probabilistic analysis can be applied to a geotechnical problem by combining FE models and statistical methods. It is done by introducing the problem's parameters as a random variable resulting from geotechnical site investigation or past experience. However, to the authors' knowledge, the direct introduction of random variables in geotechnical finite element software is generally not supported in commercial codes. In this paper, finite element-based probabilistic and Bayesian inverse analyses could be carried out due to the coupling between ZSOIL.PC (2020) and UQLab (Marelli and Sudret, 2014). Based on Sudret (2007), Rocquigny et al. (2008) and Li et al. (2021), the global methodology illustrated in Fig. 1 is applied in this study. (A) Based on specific quantities of interest, an appropriate finite element model is chosen, and its solution is approximated by an accurate metamodel. (B) Based on geotechnical tests, experience and literature, the FE model parameters are characterized as probability density functions. Then, a sensitivity analysis of the parameters is performed to reduce the dimension of the random vector defined as the prior. (C) A reliability analysis based on the Monte Carlo method is performed to express the model response as a probability density function. The probability of failure of the system is calculated according to previously set thresholds. (C)' Based on in situ measurements, an inverse Bayesian analysis is performed to reduce model parameter uncertainties. Then, Steps C and C' are repeated until the model is calibrated with the in situ measurements. This scheme is very general, and some steps can be further extended for practical applications. Combining metamodelling, sensitivity analysis, observational methods, sequentially driven Bayesian analyses and risk analysis, this scheme can help in decision-making and in optimizing designs during construction (Straub and Papaioannou, 2015; Wang et al., 2016; Wagner et al., 2021).

We first consider a geotechnical problem whose mechanical behaviour can be represented by an FE model denoted $\mathcal{M}$:

$$\boldsymbol{X} \in \mathcal{D}_X \subset \mathbb{R}^M \mapsto Y = \mathcal{M}(\boldsymbol{X}) \in \mathbb{R} \tag{1}$$

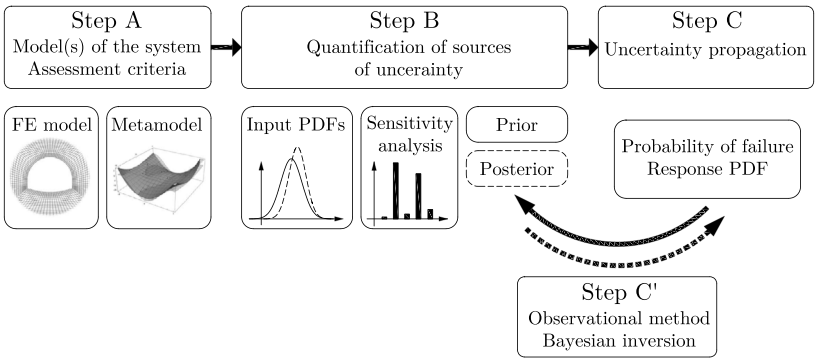

Fig. 1. Visual representation of the global theoretical framework for uncertainty quantification.

where $\boldsymbol{X} = \{x_1, \ldots, x_M\}$ is a random vector including the M probabilistic input parameters of the problem and Y gathers the output quantity, which is also called the quantity of interest (QoI). If multiple quantities of interest are contained in the output, $\boldsymbol{Y} \in \mathbb{R}^q$ is defined as a vector with q components.

2.1. Metamodelling

Any Monte Carlo-based analysis usually requires a large number of model evaluations. When this approach is chosen, the size of the input set must be large to ensure sufficient accuracy. Running the model many times causes the MCS method to be particularly unsuitable even for simple finite element models. To solve this problem, *metamodels* (also called *surrogate models* or *approximation models*) can be used to replace the original FE model with an easy-to-evaluate model, such as analytical expressions in closed forms. Since the first interpolation and regression methods (Krige, 1951; Ghanem and Spanos, 1991) were performed on numerical models, metamodelling techniques applied to geotechnical problems have been widely used over the years (Zhang et al., 2020a).

2.1.1. Polynomial Chaos Kriging (PCK)

Schöbi et al. (2015) showed that the coupling between Kriging (interpolation) and PCE — Polynomial Chaos Expansion (regression) could lead to a more accurate approximation of the original model response. This approach is called polynomial chaos kriging (PCK). More recently, Zheng et al. (2023) have shown that PCK is more accurate than Kriging or PCE in predicting displacements caused by tunnel excavation modelled by the finite element method, hence the use of PCK for the approximation model in this paper. The global and local behaviour is captured by combining orthonormal polynomials $\Psi_{\boldsymbol{\alpha}}(\boldsymbol{X})$, which describe the trend of the kriging, and the zero-mean, unit-variance stationary Gaussian process $\sigma^2 Z(\boldsymbol{X}, \omega)$. The formulation of the PCK is then obtained by

$$Y \approx \widehat{Y}_{\mathrm{PCK}} = \widehat{\mathcal{M}}_{\mathrm{PCK}}(\boldsymbol{X}) = \sum_{\boldsymbol{\alpha} \in \mathcal{A}} y_{\boldsymbol{\alpha}} \Psi_{\boldsymbol{\alpha}}(\boldsymbol{X}) + \sigma^2 Z(\boldsymbol{X}, \omega) \tag{2}$$

2.1.2. PCK-error assessment

A proper way to verify the accuracy of a PCK is by a validation set-based error. However, since this method requires additional model evaluations that can be computationally expensive for complex simulations, this option is excluded in the present study. Another method consists of an experimental design-based error called the leave-one-out (LOO) error. Since the PCK is a simple Kriging with an advanced trend, the standard LOO error formulation for Kriging models can be applied to quantify its accuracy. The LOO error is expressed in the following form:

$$\mathrm{err}_{LOO}^{(\mathrm{PCK})} = \frac{\mathrm{Err}_{LOO}^{(\mathrm{PCK})}}{\mathrm{Var}[\mathcal{Y}]} = \frac{\sum_{i=1}^{N} \left[\mathcal{Y}^{(i)} - \mu_{\hat{Y}(-i)}\left(\boldsymbol{\mathcal{X}}^{(i)}\right)\right]^2}{\sum_{i=1}^{N} \left[\mathcal{Y}^{(i)} - \hat{\mu}_{\mathcal{Y}}\right]^2} \tag{3}$$

where $\mu_{\hat{Y}(-i)}(\boldsymbol{\mathcal{X}}^{(i)})$ is the prediction mean at the sample $\boldsymbol{\mathcal{X}}^{(i)}$ by a PC-Kriging-based metamodel built on the reduced experimental design $\boldsymbol{\mathcal{X}}^{(-i)}$.

2.2. Sensitivity analysis

The aim of a sensitivity analysis is to describe how the variability of the model response Y is affected by the variability of the input parameters $\boldsymbol{X}$. In a purely numerical consideration, the sensitivity analysis may considerably improve the calculation time by reducing the number of random variables of the problem. Furthermore, in an engineering context, the sensitivity may help the modeller identify the most impacting input variables on the model behaviour. Several methods are available to perform such an analysis. To discuss both the case of independent and dependent variables, Sobol' and Kucherenko methods are used in this study.

2.2.1. Sobol'-based sensitivity analysis

Sobol' indices are based on the idea that an integrable function can be decomposed into summands of different dimensions (Sobol, 2001; Marelli et al., 2021). This decomposition only holds in the case of independent input variables. The model's total variance is described in terms of the sum of the variances of the summands. The total Sobol' indices are defined as the sum of the *higher-order Sobol' indices*, which represent the relative contribution of each group of variables $\{X_{i_1}, \ldots, X_{i_s}\}$ to the total variance:

$$S_i^T = \sum_{i \subset \{i_1, \ldots, i_s\}} \frac{D_{i_1, \ldots, i_s}}{D} \tag{4}$$

2.2.2. Kucherenko-based sensitivity analysis

Regarding the case of dependent variables, Kucherenko et al. (2012) proposed a way to define sensitivity indices directly by decomposing the output variance with the law of total variance, which enables a generalization of the Sobol' method applicable for dependent input variables.

2.3. Reliability analysis

A limit state is defined as the state beyond which a system no longer satisfies some performance measure (ISO 2394, 2015). A system represented by a random vector $\boldsymbol{X} \in D_{\boldsymbol{X}} \subset \mathbb{R}^M$ is considered. Two subsets D_s (safety domain) and D_f (failure domain) can be defined such that $D_s, D_f \subset D_{\boldsymbol{X}}$. These two domains represent the safety and failure regions delimited by the hypersurface $g(\boldsymbol{X})$, which is also called the limit state function that assumes positive values in the safe region and negative values in the failure region. Numerically, the distinction between the safety and failure domains is introduced by the *indicator function of the failure domain*:

$$\mathbf{1}_{D_f}(\boldsymbol{x}) = \begin{cases} 1 & \text{if } g(\boldsymbol{x}) \leq 0 \Leftrightarrow \boldsymbol{x} \in D_s \\ 0 & \text{if } g(\boldsymbol{x}) > 0 \Leftrightarrow \boldsymbol{x} \in D_f \end{cases}, \boldsymbol{x} \in D_{\boldsymbol{X}} \tag{5}$$

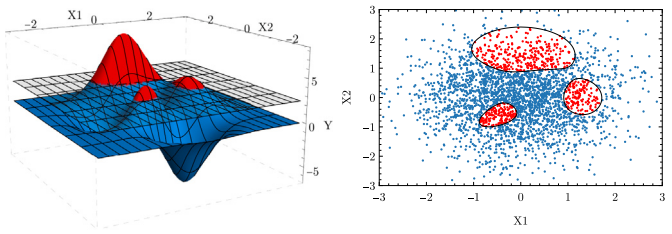

(a) Peaks function (b) Safe and failure domains

Fig. 2. Illustration of the concepts described in Section 2.3. The safety (blue) and failure (red) domains are defined by the surface $g(\boldsymbol{X})$ (gray)

Table 1
Empirical rules for the size of the sampling set N.

Type of computation	Size of sampling set N
Moments or PDF	$\sim 10^3$
Sensitivity indices	$\sim 10^4$ or ^{5}
Probability of failure $P_f \approx 10^{-k}$	$\sim 10^{k+2}$

2.3.1. Monte Carlo simulation (MCS)

Because of its statistically robust formulation, general convergence and simple formulation, Monte Carlo simulations (MCS) are emphasized and used in this paper. In this context, the empirical probability of failure $\widehat{P}_f$ is computed directly by covering the input domain with a large sample set. Given a sample size N of the input random vector $\boldsymbol{X}$, the empirical probability of failure $\widehat{P}_f$ can be obtained by Eq. (6).

$$\widehat{P}_f = \frac{1}{N}\sum_{k=1}^{N} \mathbf{1}_{\mathcal{D}_f}\left(\boldsymbol{x}^{(k)}\right) = \frac{N_{fail}}{N} \tag{6}$$

To illustrate Eq. (6), Fig. 2(a) shows the well-known peak function with a failure domain defined by $g(\boldsymbol{X}) = 2.5 - \mathcal{M}^{\text{Peaks}}(\boldsymbol{X})$. Given two standard normally distributed variables (X_1, X_2), Fig. 2(b) is obtained by successively evaluating the model according to these two random variables.

Since the convergence rate of the MC method is approximately proportional to $\propto 1/\sqrt{N}$ and considering a confidence interval of 5%, the rules listed in Table 1 can be applied to the sample size to ensure sufficient accuracy (Sudret and Commend, 2021):

2.3.2. Adaptive Kriging Monte Carlo simulation (AKMCS)

Metamodels accurately predict the original model response in the vicinity of the experimental design samples. When the original model is highly nonlinear or/and the target probability of failure has a low magnitude, these experimental design samples may not be optimal for estimating the probability of failure with sufficient accuracy. The AKMCS method solves this problem through an adaptive experimental design that automatically generates more points in the neighbourhood of the limit state function $g(\boldsymbol{x}) = 0$, thereby increasing the local quality of the metamodel (Echard et al., 2011; Marelli and Sudret, 2021). The probability of failure is then computed with Eq. (6). The PCK is a standard Kriging with an advanced trend, and the AKMCS algorithm remains applicable. Moreover, Schöbi et al. (2017) showed that its use can significantly improve the convergence of the algorithm.

2.4. Bayesian analysis

Furthermore, the Bayesian analysis allows updating uncertainties of the input parameters by inputting measurements into the model. More precisely, the goal is to quantify how the *prior* has to be updated for a match between the model response and the measurement set $\mathcal{Z} = \{z_1, \ldots, z_N\}$. To link the predictions with the observations and to numerically solve the inverse solution, Eqs. (1) and (2) must be extended by an additive *discrepancy* term noted $\boldsymbol{\varepsilon}$. The simplest form

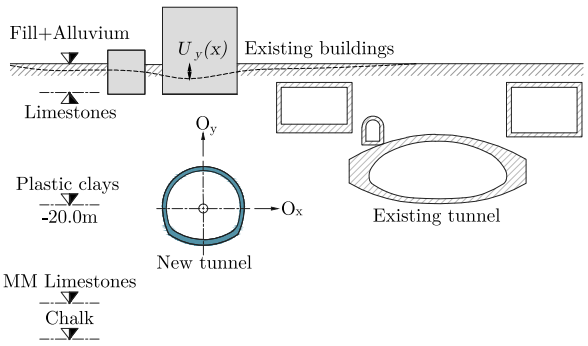

Fig. 3. Simplified cross-section geometry of the project and quantity of interest.

is a zero-mean Gaussian with a standard deviation $\boldsymbol{\Sigma}$. The observations can then be approximated by

$$Z \approx Y + \varepsilon \approx \widehat{\mathcal{M}}_{\text{PCK}}(\boldsymbol{X}) + \varepsilon \quad \text{where} \quad \varepsilon \sim \mathcal{N}(0, \Sigma) \tag{7}$$

Due to the information provided by on-site measurements, it is possible to switch from the distribution of the output to the distribution of the output *given* the observation and then to the distribution of the input *given* the observation $f_{\boldsymbol{X}}(\boldsymbol{X} \mid Z)$, which is given by Bayes' theorem:

$$f_{\boldsymbol{X}}(\boldsymbol{X} \mid Z) = a \cdot f_{\boldsymbol{X}}(\boldsymbol{X}) \cdot \mathcal{L}(\boldsymbol{X}, Z) \tag{8}$$

where $f_{\boldsymbol{X}}(\boldsymbol{X})$ is the prior probability density function and the constant $a^{-1} = \int_{-\infty}^{\infty} \mathcal{L}(x) f_{\boldsymbol{X}}(x) dx$ is the normalizing constant that ensures that the posterior distribution $f_{\boldsymbol{X}}(\boldsymbol{X} \mid Z)$ integrates to 1. If the observations are statistically independent, the likelihood $\mathcal{L}(\boldsymbol{X}, Z) = \prod_{i=1}^{N} f_{\boldsymbol{X}}(z_i \mid x)$ is the joint probability of observing Z given $\boldsymbol{X}$. One measurement z_i is considered. Because of the additive discrepancy described in Eq. (7), the likelihood function of $\mathcal{M}(\boldsymbol{X})$ is a Gaussian distribution centred on the measurement z_i such that the posterior distribution in Eq. (8) becomes

$$f_{\boldsymbol{X}}(\boldsymbol{X} \mid Z) = a \cdot f_{\boldsymbol{X}}(\boldsymbol{X}) \cdot \prod_{i=1}^{N} \mathcal{N}(z_i \mid \mathcal{M}(\boldsymbol{X}), \boldsymbol{\Sigma}) \tag{9}$$

Since Eq. (9) does not have a closed form solution for most practical cases, numerical methods are involved. The numerical method used in this paper to solve the inversion is the Markov Chain Monte Carlo (MCMC) method with the Affine Invariant Ensemble Sampling (AIES) algorithm (Goodman and Weare, 2010; Wagner et al., 2021). To assess the algorithm's convergence, Gelman and Rubin (1992) proposed a method to compare the within-chain and between-chain variances. This method, called the Gelman–Rubin diagnostic, is used later in this article.

3. White House Station - Case study description

The case study applying the probabilistic approach addresses a tunnel in the Grand Paris Express project. This tunnel is located at the future White House Station on Line 14 of the Paris Metro (**GoogleEarth**). The project is characterized by a dense urban environment with sensitive and vulnerable existing neighbouring structures. Geotechnical investigations were carried out during the geotechnical studies of the G1, G2 and G3 missions per the standard (AFNOR, 2014). In total, 25 core drillings, 13 pressuremeter tests, 2 dilatometer tests, 1 cross-hole test, 21 destructive drills and 5 static penetrometer drills were carried out on an area of 5690 m^2, i.e., 1 test per 73 m^2. Furthermore, numerous identification tests and mechanical property measurements were performed in the laboratory (Zhang et al., 2020b, 2022). The soil is composed of 6 different soil layers, including plastic clays between two harder limestone layers located at the level of the new tunnel. Fig. 3 shows the simplified cross-section geometry of the project.

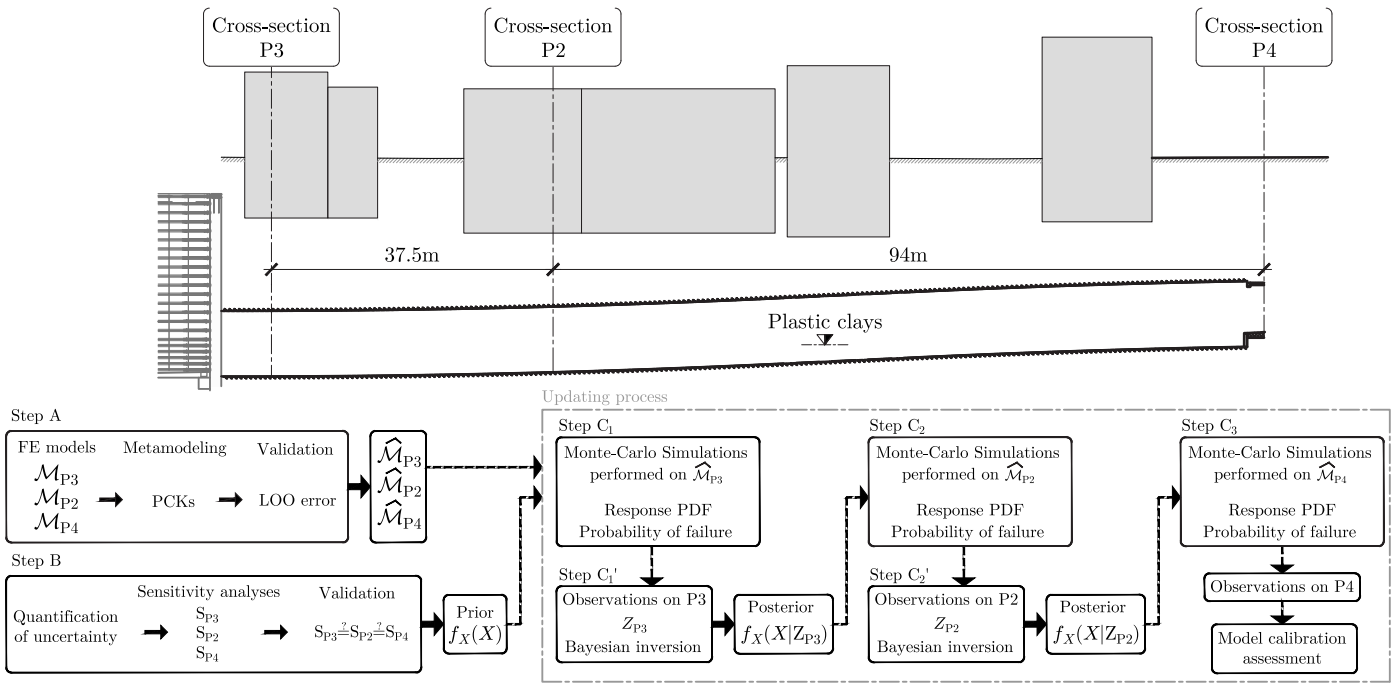

Fig. 4. Flow chart of the process used for probabilistic analysis of the White House Station project.

3.1. Calculation approach

Fig. 4 shows the longitudinal section of the tunnel with the calculation steps corresponding to the procedure illustrated in Section 2. Further explanations are given hereafter:

(A) We selected three cross-sections P3, P2, and P4 to develop three finite element models using ZSOIL software. Thereafter, we generated a dataset to train the PC-Kriging metamodel and verified the adequacy of the training set by computing the leave-one-out error for each model.

(B) The mean values of the probability density distributions were established based on geotechnical laboratory tests. Selecting the types of distributions and standard deviations was based on relevant literature and our expertise. Using these distributions, we performed sensitivity analyses on the P3, P2, and P4 cross-sections to ensure that they were influenced by the same set of parameters. The variables that had no effect on the model response were fixed at their mean values, while the impacting variables were treated as random variables. The resultant random vector was defined as the prior.

(C_1) Using the prior distributions, we conducted reliability analyses via PCK-based Monte Carlo and adaptive PC kriging Monte Carlo simulations. We established the probability density response of the model and computed the associated probability of failure according to pre-set thresholds.

(C_1') In situ observations of surface settlements were used to perform the first inverse Bayesian analysis to reduce the uncertainties of the prior distributions, resulting in a new posterior random vector.

($C_i \leftrightarrow C_i'$) We repeated the procedure by communicating the C and C' steps. We compared the predictions in the form of a probability density with the observations until the model was calibrated. Regarding the present case study, the procedure had to be repeated twice for sufficient calibration.

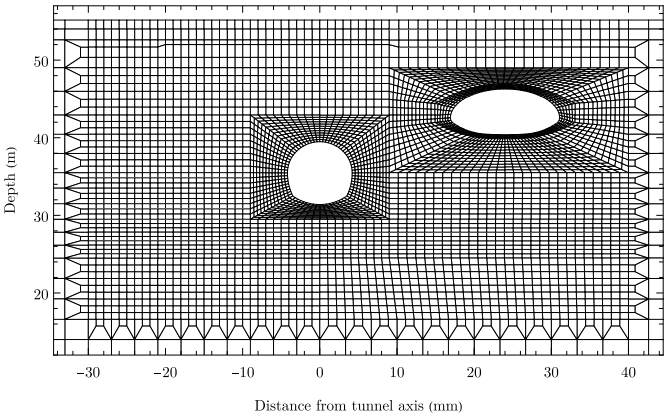

Fig. 5. FE mesh of the P3 cross-section generated in ZSOIL.

3.2. Constitutive laws and mesh

The cross-section geometry was meshed with three sizes of linearly interpolated quad elements: 0.5×0.5 m in the vicinity of the tunnels, 1.0×1.0 m over a distance of -30 m resp. 40 m from the axis of the new tunnel, and then 2.0×2.0 m. The three models were subject to a mesh sensitivity test. Specifically, the mesh size used in the models was divided by a factor of two, and the resulting output quantities such as surface settlement, tunnel convergence, and lining bending moments were compared to those obtained from the original mesh size, as shown in Fig. 5. The results showed an average difference of 2.5% between the two mesh sizes, which we deemed an acceptable level of variation. Consequently, we proceeded to perform the subsequent calculations using the original mesh size illustrated in Fig. 5. The constitutive laws used for modelling the soil behaviour were the Hardening Soil with Small strain extensions (HSS) (Obrzud and Truty, 2010) and standard Mohr–Coulomb (SMC) models. The HSS model is highly suitable for handling small deformations at the serviceability limit state (Kawa et al., 2021). The choice of the constitutive laws and their parameters in mean value is given in Table 2. Since the aim is to determine the surface

Table 2
Main geomechanical parameters (mean values) of the constitutive laws and their assumed parameter distributions.

Formation		Model	Situation	Stiffness	Resistance			Stress state		
				$E_{50} = E_{oed} = \frac{1}{3}E_{ur}$ (MPa)	c (kPa)	φ (°)	ψ (°)	$K_0 = 1 - \sin(\varphi)$ (–)	ν_{ur} (–)	m (–)
Statistical distribution Coefficient of variation				Lognormal CV = 40%	Lognormal CV = 20%	Lognormal CV = 10%		Deterministic -		
Fill		HSS	Drained	15	0	33	3	0.53	0.2	0
Alluvium		HSS	Drained	12	14	27	0	0.61	0.2	0
Limestones	Upper	HSS	Drained	50	8	38	8	0.47	0.2	0
	Medium	SMC	Drained	300	85	45	15	–	–	–
	Lower	SMC	Drained	400	141	54	24	–	–	–
Plastic clays	Upper	HSS	Undrained	20	$c_u = 141$	0	0	0.72	0.49	0
	Medium	HSS	Undrained	42.5	$c_u = 191$	0	0	0.72	0.49	0
	Lower	HSS	Undrained	65	$c_u = 240$	0	0	0.72	0.49	0
Limestones Marly Meudon		SMC	Drained	75	21	38	8	–	–	–
Chalk		SMC	Drained	500	57	41	11	–	–	–

settlements during the tunnel excavation, the short-term behaviour (drained/undrained) should be considered for each soil layer according to their corresponding permeability. The assumed short-term behaviour of each layer is given in Table 2.

3.3. Quantity of interest and failure criterion

The quantity of interest of the problem is the settlement at the ground surface, more precisely, the vertical displacement $U_y(x)$ over a distance of 20 m on both sides of the axis of the new tunnel. The failure of the system was considered when the surface settlement exceeded $|U_{y,adm}| = 10$ mm. Formally, the failure state is then defined as:

$$g(x) = U_{y,adm} - \max(|U_y(x)|) \tag{10}$$

3.4. Quantification of uncertainties

In practice, field tests rarely allow the determination of a proper statistical distribution, including a standard deviation due to an insufficient number of on-site investigations. However, the available literature provides a target distribution and target coefficient of variation for some geotechnical parameters (Duncan, 2000; Baecher and Christian, 2003; Kayser and Gajan, 2014; Phoon and Ching, 2018). The coefficient of variation could also be determined based on the experience of other investigations carried out in the vicinity of the project. The statistical distributions of the soil parameters are gathered in Table 2. The other model parameters' distributions are given in Table 3. The moments of the static loads are not provided; however, since they are variables along the longitudinal axis of the tunnel, the corresponding coefficient of variation is chosen as CV=10 % (Zhao and DeJong, 2023). When considering probabilistic analyses, discussing the correlation of soil parameters is still relevant. In many practical cases, it is usual to neglect these correlations, since they introduce an additional unknown parameter (correlation matrix) that is generally not quantified by geotechnical tests. However, there are many examples in the literature that provide target values to consider the dependence between the angle of friction and cohesion (Duncan, 2000; Papaioannou and Straub, 2012; Huang et al., 2014; Zevgolis et al., 2018; Guo and Dias, 2020).

Two cases were therefore treated in the current study. In the first case, the intra-parameter dependence is ignored, and a Sobol' sensitivity analysis can be performed. In the second case, the correlation between the friction angle and the cohesion is considered and a sensitivity analysis using the general Kucherenko method is used. These points lead to an initial problem with 34 random variables, which may be reduced after performing the sensitivity analysis Appendix.

Table 3
Statistical distributions of the model parameters and their moments.

Parameter		Distribution	
Friction angle	φ	Lognormal	$\sim \mathcal{LN}$(Table 2)
Cohesion	c'	Lognormal	$\sim \mathcal{LN}$(Table 2)
Young-modulus	E	Lognormal	$\sim \mathcal{LN}$(Table 2)
Water table height	h_w	Gaussian	$\sim \mathcal{N}(29.0, 0.43)$
Static building load	F	Gumbel	$\sim \mathcal{G}(\mu, 0.1\mu)$
Confinement loss	λ		See Section 3.5

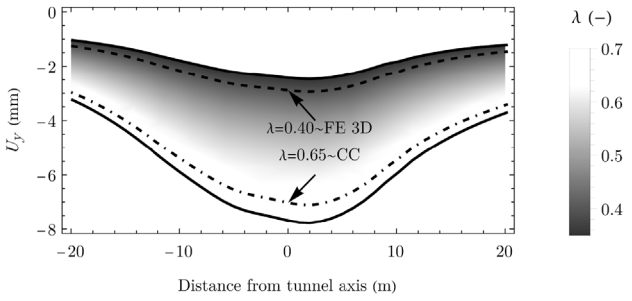

Fig. 6. Settlement field for various values of λ.

3.5. Confinement loss λ

Initially, it was envisaged to perform the probabilistic analysis directly and exclusively on the 3D model. However, since the model contains more than 420,000 nodes and 40 calculation steps, the computation time would have been too long. To show the applicability, a single deterministic 3D comparison was carried out. Alternatively, the three-dimensional effects could be estimated by the convergence confinement method (CC method), which is widely used in conventional tunnelling. The radial displacement of the tunnel is given as a function of a fictitious pressure p_i (Eq. (11)). This pressure then tends to zero as soon as the tunnel face gets closer to a particular cross-section.

$$p_i = (1 - \lambda)\,\sigma_0 \tag{11}$$

Full-face excavation was carried out with 1.0 to 1.2 m passes, and the temporary support was a HEB200 profile with 0.3 m thick shotcrete. The convergence confinement method induced a value of $\lambda = 0.65$, while the 3D model provided a value close to $\lambda = 0.4$, which was obtained by setting the confinement loss before installing the temporary support in the 2D model to obtain equivalent displacements on the surface in the 3D model. Fig. 6 shows the influence of λ on the response of the 2D model U_y. Instead of deterministically fixing the value of λ, λ was maintained as a random variable that is defined by an assumed

Table 4
Measured settlements on cross-section P3, P2 and P4 during the monitoring phase.

Distance from O_x (m)	−15	−9.6	−9.3	−8.9	0	10.0	15.0
Z_{P3} (mm)	−4.00	−5.7	−5.9	−6.1	−6.9	−5.5	−3.5
Distance from O_x (m)				−8.1	0	18.1	
Z_{P2} (mm)				−6.0	−6.8	−3.9	
Distance from O_x (m)	−13.3	−11.6	−3.3	0	3.2	11.7	13.2
Z_{P4} (mm)	−1.6	−1.7	−2.9	−3.7	−2.9	−1.7	−1.6

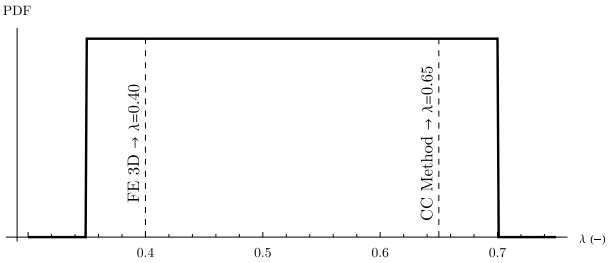

Fig. 7. Probability density function of the parameter λ; the dashed lines represent the values calculated with the 3D model and the CC method.

uniform distribution $\lambda \sim \mathcal{U}(a, b)$. The distribution parameters were set according to the values obtained by the 3D model and the CC method with an error of 10%, which led to $a = 0.35$ and $b = 0.7$. The corresponding uniform distribution is shown in Fig. 7.

3.6. Model discrepancy and measurement data

According to Eq. (7), using a model as a predictor requires the addition of a discrepancy term. Quantifying this error is not easy in practice, so we first separate the measurement error $\boldsymbol{\varepsilon}_{\mathcal{Z}}$, the original model error $\boldsymbol{\varepsilon}_{\mathcal{M}}$ and the metamodel error $\boldsymbol{\varepsilon}_{\widehat{\mathcal{M}}}$:

$$\boldsymbol{\varepsilon} = \boldsymbol{\varepsilon}_{\mathcal{Z}} + \boldsymbol{\varepsilon}_{\mathcal{M}} + \boldsymbol{\varepsilon}_{\widehat{\mathcal{M}}} \tag{12}$$

$\boldsymbol{\varepsilon}_{\mathcal{Z}}$ was quantified directly by the company in charge of the surveys. In this case, a tolerance of ±1 mm was considered (taking into account the direct measurement error as well as the "breathing" of the building material generated by the temperature gradients during the monitoring and construction phase). Since this tolerance was absolute and did not depend on the location or the measured value (no local and size effects), the measurement error was defined by considering a 5% and 95% confidence interval and reads for all measurements $\boldsymbol{\sigma}_{\boldsymbol{\varepsilon}_{\mathcal{Z}}} = \mathbf{0.6}$.

$\boldsymbol{\varepsilon}_{\mathcal{M}}$ was selected based on personal judgement. The error was related to the magnitude of the measured settlements with a coefficient of variation $\mathrm{CV}_{\boldsymbol{\varepsilon}_{\mathcal{M}}} = 0.15 \rightarrow \boldsymbol{\sigma}_{\boldsymbol{\varepsilon}_{\mathcal{M}}} = \mathrm{CV}_{\boldsymbol{\varepsilon}_{\mathcal{M}}} \cdot \boldsymbol{Z}$. This covers errors related to the elements of the model (typically the mesh size, the simplification of the stratigraphy, etc.)

Table 5
PCKs specifications.

$\widehat{\mathcal{M}}_{\mathrm{PCK}}$	$\mathcal{Y}$ size	T_{FE} (hours)	$\mathrm{err}_{LOO}^{(\mathrm{PCK})}$ (−)
Cross-section P3	300	15.8	4.8×10^{-6}
Cross-section P2	300	21.2	6.1×10^{-6}
Cross-section P4	300	14.4	6.9×10^{-6}

$\boldsymbol{\varepsilon}_{\widehat{\mathcal{M}}}$ was considered to be zero. In other words, the error caused by the metamodel was considered negligible. This assumption was confirmed when testing the accuracy of the metamodels.

During each construction phase, real-time monitoring of the structures and ground was conducted. The monitoring system was established and implemented before construction began, which allowed the influence of environmental effects such as temperature to be measured. Regarding structures and ground, 11 theodolites, 1100 targets, 460 m of optical fibres, 25 inclinometers and extensometers were set up. Monitoring results during the excavation stages P3, P2 and P4 are listed in Table 4. Bayesian inversions were performed on these measurements.

4. Results and discussion

4.1. Deterministic simulations

Before applying probabilistic calculations to our numerical models, deterministic analyses were performed with the mean values listed in Table 2 and $\lambda = 0.65$. The vertical displacement fields of the cross-sections P3, P2 and P4 are presented in Fig. 8. In this analysis, the P2 cross-section model yields more surface settlement than P3 and P4.

4.2. Metamodelling and verifications

Three hundred input samples following the distributions in Table 3 were randomly and sequentially generated on a single machine and evaluated by the FE model for each cross-section constituting the initial experimental designs. This allowed the creation of 3 PCKs whose characteristics are contained in Table 5. The parameter T_{FE} represents the time needed by the FE software to generate the N points of the experimental designs $\{\mathcal{Y}_{P3}, \mathcal{Y}_{P2}, \mathcal{Y}_{P4}\}$. Based on the magnitude of the LOO errors listed in Table 5, we concluded that the original experimental design gathering 300 sample points was sufficiently large to

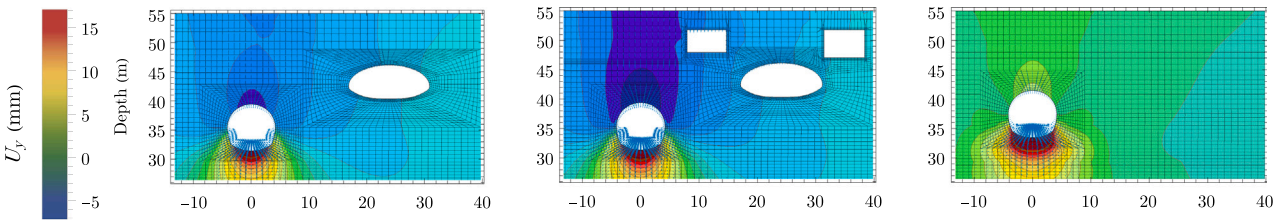

(a) Cross-section P3 (b) Cross-section P2 (c) Cross-section P4

Fig. 8. Deterministic FE simulation of vertical soil displacements with prior mean values and $\lambda = 0.65$.

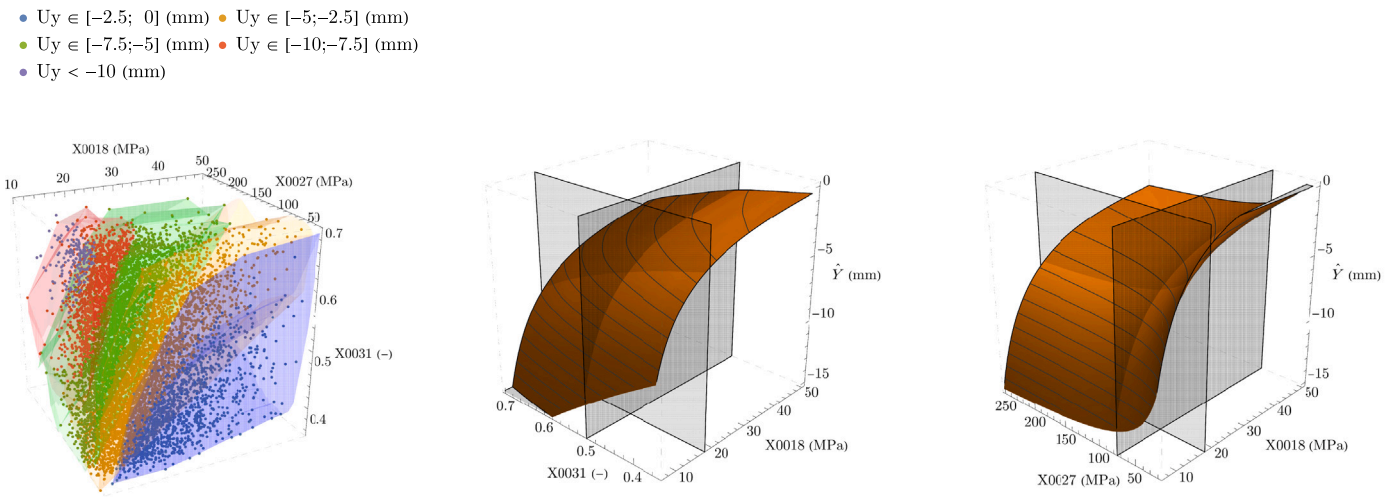

(a) PCK approximation (b) First projection (c) Second projection

Fig. 9. (a) Density plot of the PCK metamodel ($\mathbb{R}^3 \to \mathbb{R}$). (b) Isometric view of the metamodel projection on the variables X0018 and X0031 ($\mathbb{R}^2 \to \mathbb{R}$); X0027 is set to its mean value. (c) Isometric view of the metamodel projection on X0018 and X0027 ($\mathbb{R}^2 \to \mathbb{R}$); X0031 is set to its mean value.

confidently approach the solutions of the original FE models. This result allowed validation of the assumption made in Section 3.6 relative to the discrepancy of the metamodels. Furthermore, the magnitude of the LOO errors shows that we could have generated fewer sample points to achieve sufficient accuracy.

The metamodel response of the cross-section P3 ($x = 0$) is presented in Fig. 9(a) as a density plot. To interpret this figure, we chose to project the response onto a reduced two-parameter space by setting the remaining variable to its mean value. Vertical planes fixed to the mean values have been added to Figs. 9(b) and 9(c) to illustrate the higher gradient for small changes in X0018 than those generated by X0027 and X0031. The resulting Figs. 9(b) and 9(c) show the non-linearity of the approximation response and its characteristic smoothness. Here, smoothness is understood to mean a noiseless model response. Furthermore, we have interpreted Figs. 9(b) and 9(c) as a qualitative way of interpreting the sensitivity analysis conducted in Section 4.3.

4.3. Sensitivity analysis

Considering the initial 34 random variables of the problem Appendix, the PCK-based Sobol and Kucherenko sensitivity analyses over the QoI lead to the result shown in Fig. 10(a). According to Table 1, we chose a sample size of $N = 5 \times 10^4$ for estimating the indices through Monte Carlo simulation. Fig. 10(b) shows the convergence of the Total Sobol' indices depending on the MC-sample size for the three more impacting input parameters. We see that convergence is reached even before $N = 5 \times 10^4$.

Since the QoI is a curve $U_y(x)$, we chose to represent the sensitivity indices in the form of a gradient varying according to the distance from the origin O_x. Fig. 10(a) shows that regardless of the position of the settlement, the model response is always influenced by the same input parameters. As described in Fig. 4, such sensitivity analyses have been carried out on each cross-section to ensure that the parameters are not strongly influenced by its geometry and by the static loads generated

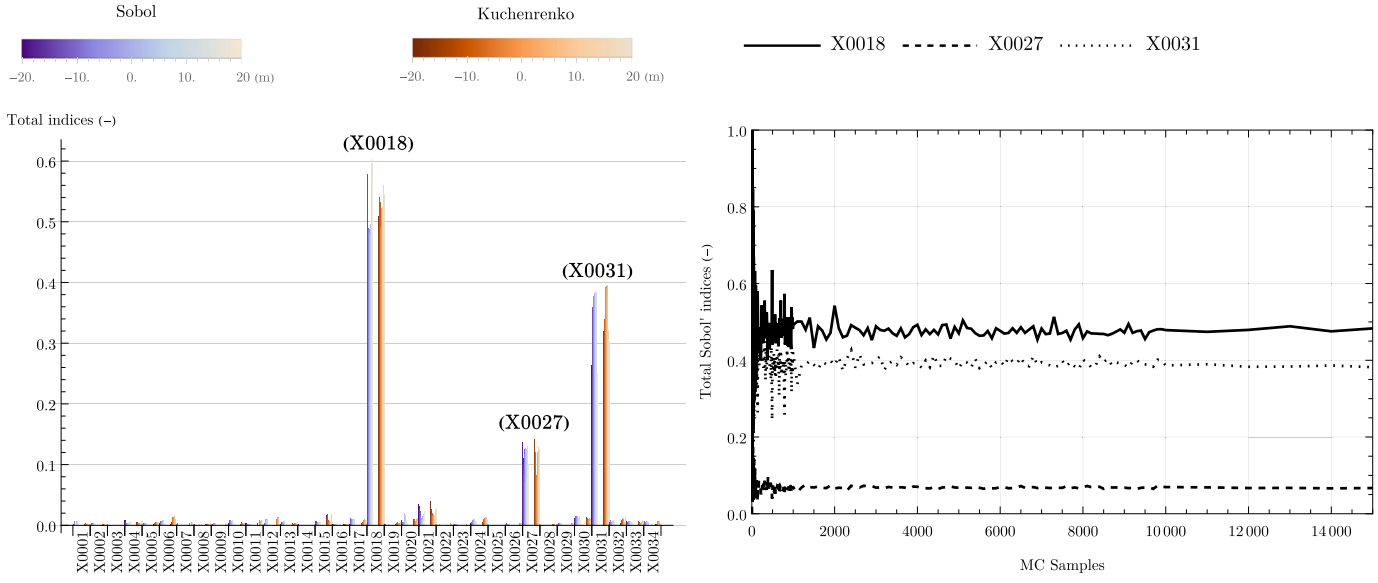

(a) Sensitivity analysis of the cross-section P3 (b) Convergence of Sobol' indices

Fig. 10. (a) Bar chart showing the sensitivity analyses from a PCK-based Sobol decomposition (case of independent variables) and Kuchenrenko's generalized method (case of dependent variables). (b) Convergence of the Total Sobol' indices estimation for some chosen input variables at a distance $x = 0$ m.

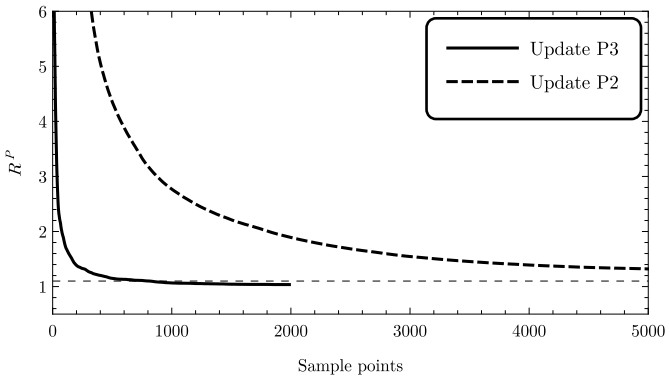

Fig. 11. History of the Gelman–Rubin diagnostic of the two inversions.

by neighbouring buildings. The three sensibility analyses performed on the cross-sections P3, P2 and P4 provided a similar outcome to that shown in Fig. 10(a).

More exhaustively, the three parameters that most influence the QoI are:

(X0018) Young's modulus of the upper layer of the plastic clays,
(X0027) Young's modulus of the Marly Meudon limestone,
(X0031) Confinement loss λ.

These results showed that the stiffness parameters mainly influenced the response of the model in a displacement problem. Similar results were observed by Papaioannou et al. (2013) and Miro et al. (2014) in slightly different cases of tunnel studies using hardening constitutive models. The small influence of the correlation between φ and c can easily be explained by the fact that both parameters have a more decisive effect on the soil *strength* than on its *stiffness*. The transformation from a three-dimensional to a two-dimensional problem also involves a strong influence of the confinement loss λ on the model response.

This sensitivity study allowed a definitive reduction of the random variables from 34 to 3. From this point, the results presented later in this paper are derived from probabilistic analyses carried out on a reduced input space of the three above input parameters, which we defined as the prior.

4.4. Bayesian analyses

The results hereafter come from 2 Bayesian inversions performed on the cross-sections P3 and P2. First, inversion (P3) was performed on 100 Markov chains containing each 2000 sample points, which enabled us to obtain apparent convergences of the Gelman–Rubin diagnostic $\hat{R}^p < 1.1$, as shown in Fig. 11. The second inversion (P2) was solved with 500 Markov chains and 15,000 sample points to reach the $\hat{R}^p < 1.1$ criteria. As shown in Fig. 11, the first inversion showed a rapid convergence, which we explain by the lack of initial correlation between the variables. Because of the correlation generated by the inference on the posterior samples of the first inversion, the high correlation (especially between the variables X0018 and X0031) on the input of the second inversion negatively affects the convergence of the Markov chains. Fig. 12 shows the evolution from prior to posterior distributions.

Inference on the posterior distributions showed that the variables X0018 and X0027 could be described according to a lognormal distribution and X0031 to a truncated Gaussian distribution bounded by the uniform prior. The values of the moments defining these distributions are listed in Table 6. The dependencies between the parameters were supported, assuming a Gaussian copula defined by the correlation matrices of the posteriors. These matrices are shown in the upper part of Fig. 12, while the associated mixed distributions are shown in the lower part. According to Table 6, the decrease in the uncertainty

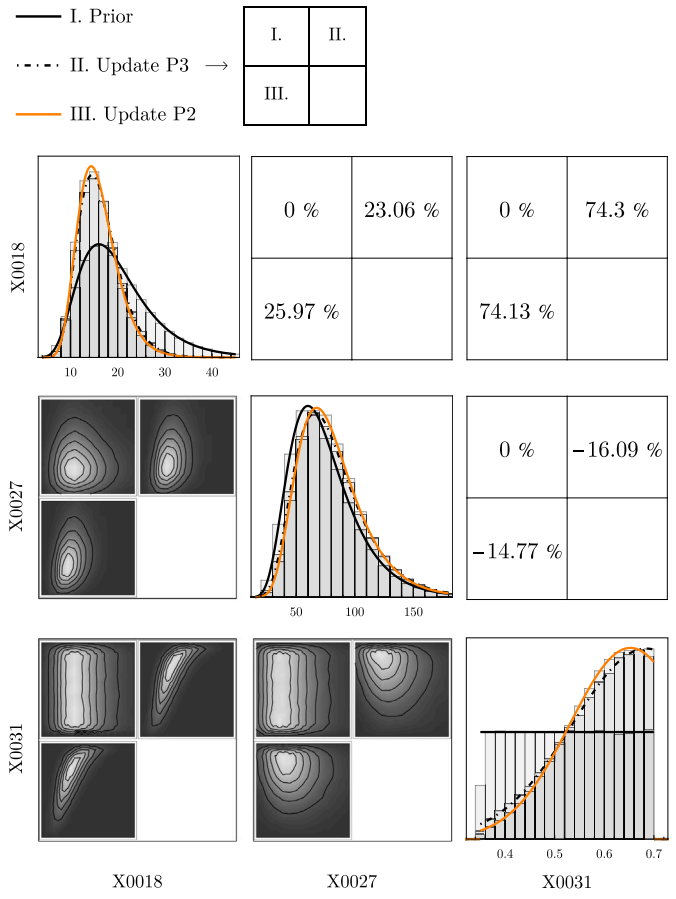

Fig. 12. Global results of the Bayesian analyses. The density plots represent the evolution of the copulas over the different updates. The numbers in the upper part of the matrix represent the evolution of the correlation between the parameters.

Table 6
Updating of the moments (mean and standard deviation) via Bayesian inversions.

Input	X0018		X0027		X0031	
	μ_X (MPa)	σ_X	μ_X (MPa)	σ_X	μ_X (–)	σ_X
Prior	20.0	8.0	75.0	30.0	0.53	0.10
Update P3	16.3	4.5	80.8	29.9	0.58	0.09
Update P2	16.1	4.2	81.6	29.6	0.58	0.08

through input refinement can be seen in the decline in the standard deviations σ_X over the inversions. We suspect the second posterior update is small because of the lack of measurements available on P2. If the prior distribution of Young's modulus of plastic clays (X0018) tends to underestimate the observed settlements, the confinement loss (X0031) will compensate for this underestimation during the Bayesian inversion, and vice versa. This is how the correlation between X0018 and X0031 can be explained.

4.5. Reliability analyses

In parallel to the Bayesian inversions and according to Fig. 4, uncertainty propagations were performed to compare the on-site measurements and the probability density function of the model response. PDF curves were generated by running $N = 10^7$ model evaluations on PCK approximation models. According to Eq. (6), the probabilities of the failure $\hat{P}_f$ were calculated directly by setting the failure function $g(x)$ to the value given in Section 3.3. They were then compared to the reference value used in Eurocode 0. For validation, the AKMCS method

Table 7
Probabilities of failure ($\widehat{P}_f$ in %) that the surface settlement exceeds 10 mm using MC ($N = 10^7$) and AKMC analysis.

Input	P3		P2		P4	
	MC	AKMC	MC	AKMC	MC	AKMC
Prior	4.05	4.01	4.36	4.60	0.06	0.07
Update P3				$<10^{-5}$		$<10^{-5}$
Update P2						$<10^{-5}$

was applied to the original FE model to ensure that the experimental design along the failure surface was sufficiently accurate. The PDF curves displayed in this section represent the settlements of the ground at a distance $x = 0$ m from the origin. Table 7 summarizes the failure probabilities for the three cross-sections. It can be seen that some values have been deliberately truncated according to the empirical rules given in Table 1. Since the sample size is $N = 10^7$, the maximum expected accuracy is of a magnitude $\widehat{P}_f > 10^{-(k-2)}$, where $k = 7$.

4.5.1. Cross-section P3

The cross-section P3 is the first phase of the tunnel excavation. The unique information contained in the prior is given by the site investigation and target values in the literature. Propagating uncertainties according to the prior's distribution led to the output distribution shown in Fig. 13(a). The mode of the model prediction is located at a settlement of −4.0 mm when the measurement was reported at −6.9 mm. Fig. 13(b) shows the convergence of the failure probability (threshold according to Section 3.3) of an AKMC simulation. According to a confidence interval of 1%, convergence was reached after 79 evaluations of the original FE model. The resulting failure probability yields the same value as the Monte Carlo analysis performed on the PCK model (see Table 7).

Through Fig. 13(a), we noticed that the numerical model underestimates the settlement. Nevertheless, the probability of exceeding −10 mm of the settlement was calculated to be 4.01%, below the 6.7% threshold proposed by the Eurocode for a 50-year duration.

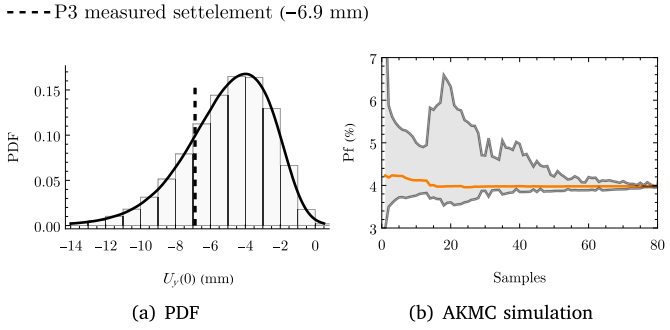

(a) PDF (b) AKMC simulation

Fig. 13. (a) Probability density function from Monte Carlo simulation. (b) AKMC analysis yielding a convergence at $P_f = 4.01\%$.

4.5.2. Cross-section P2

Fig. 14(a) contains two predictions: the first prediction comes from the prior, and the second prediction comes from the posterior associated with the inversion performed on the cross-section P3. The modes of the distributions are $\text{Mo}_{\text{Prior}} = -4.0$ mm and $\text{Mo}_{\text{UpdateP3}} = -6.85$ mm, respectively. Fig. 14(b) shows the cumulative density functions for several thresholds $U_{y,\text{adm}}$.

On the cross-section P3, we noticed that the model underestimates the settlements. As shown by the deterministic analyses illustrated in Fig. 8, the cross-section P2 is the most critical in terms of surface movements. Reflections based on the deterministic analyses may have led to reinforcement actions to ensure that settlement does not exceed −10 mm. However, after refining the prior, we could train our predictor and thus ensure that the probability of exceeding the threshold settlement was close to zero. The posterior results with low probability failure allow possible optimization of supporting and lining structures (augmentation of distance between supporting profiles, reduction of profile size, etc).

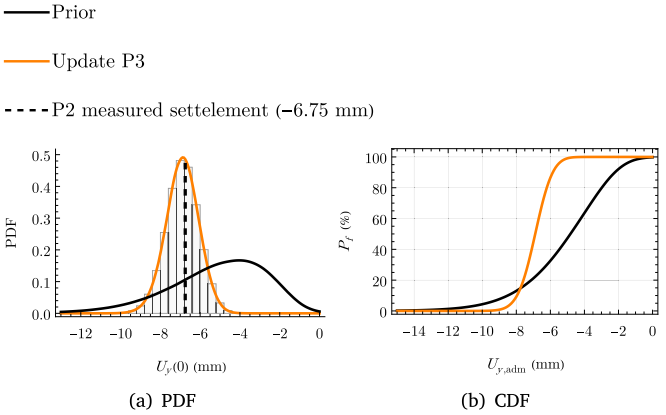

(a) PDF (b) CDF

Fig. 14. (a) Probability density function from Monte Carlo simulation. (b) Probability of failure depending on a threshold $U_{y,\text{adm}}$.

4.5.3. Cross-section P4

The cross-section P4 is located at a distance of 94 m from P2. Propagating the prior and the inversions performed on P3 and P2 yields the PDF in Fig. 15(a). The modes of the distributions are $\text{Mo}_{\text{Prior}} = -2.25$ mm, $\text{Mo}_{\text{UpdateP3}} = -3.7$ mm and $\text{Mo}_{\text{UpdateP2}} = -3.8$ mm. Thus far, we have only shown results at one particular node located at the vertical axis of the tunnel $U_y(0)$, while the quantity of interest was defined as the whole curve from $x \in [-20; 20]$ m. Fig. 15(b) introduces a probability density field of the complete settlement curve. Black marks represent the in situ measurements. The probability density component is illustrated with a colour gradient varying from 0 to 0.8.

Fig. 15 shows that the settlement prediction remains reliable with the last two updates despite the distance between the two cross-sections. This favourable result is explained by the fact that the soil stratigraphy between P2 and P4 varies only slightly with respect to the tunnel axis. However, the conclusions could be different if the thickness and height of the soil layers vary significantly.

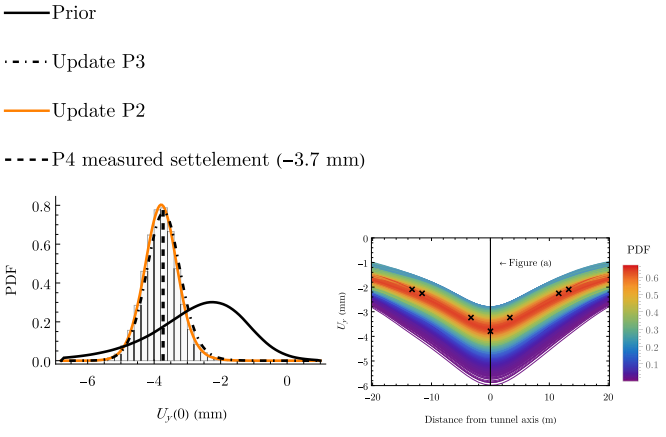

(a) PDF (b) Density plot of the scalar field

Fig. 15. (a) Particular solution of the density function field at $x = 0$ m. (b) Complete PDF field of the surface settlements for the P4 cross-section with in situ measurements according to the last posterior input.

5. Conclusion

In the present paper, a global finite element-based probabilistic framework using metamodelling is proposed. This probabilistic framework has then been applied to a real-world case study of a tunnel starting from the White House Subway Station in Paris to predict ground settlements during tunnel construction. The obtained results allow the following conclusions to be drawn:

(1) The creation of a suitable metamodel using PCK method helps limiting FE model calculations to a reasonable number of samples with good approximation results.
(2) The a priori distributions for input parameters can be determined based on geotechnical investigations results and formerly known knowledge.
(3) The presented sensitivity analyses allow to identify key input parameters. For problems with a large number of uncertain parameters, it enables a significant reduction of computation time.
(4) Probabilities of failure or reliability beta-indices can then be derived using metamodeling-powered Monte-Carlo and Adaptive Kriging Monte-Carlo Simulations methods.
(5) By means of field monitoring measurements, Bayesian inverse analyses help specify the probability that settlements exceed acceptable values by updating the a priori hypotheses. Hence, the a posteriori results are refined with a better prediction of displacements.
(6) It can be concluded from this work that the probabilistic approach using finite element method has a promising potential to enhance the reliability assessment for SLS cases, which can afterwards enrich design codes.

The proposed global probabilistic framework proves to be suitable for serviceability problems related to tunnel excavation in urban areas, not only in terms of prediction quality but also in terms of computation time, thus making it applicable for other practical applications. The next steps are to apply this framework to numerical models considering hydromechanical coupling and to larger 3D models.

CRediT authorship contribution statement

Jocelyn Minini: Conceptualization, Software, Formal analysis, Methodology, Writing – original draft. **Yi Zhang:** Investigation, Resources, Writing – original draft, Writing – review & editing, Supervision. **Marc Groslambert:** Methodology, Writing – review & editing. **Stéphane Commend:** Project administration, Funding acquisition, Data curation, Resources, Supervision, Validation.

Declaration of competing interest

The authors declare that they have no known competing financial interests or personal relationships that could have appeared to influence the work reported in this paper.

Data availability

Data will be made available on request.

Acknowledgments

The authors would like to thank Prof. **Thomas Zimmermann**, Prof. **Bruno Sudret**, Dr. **Stefano Marelli**, Prof. **Jean-Pierre Magnan**, Dr. **François Toutlemonde** and Prof. **Jean-Armand Calgaro** for the discussions about the applications of FE probabilistic approaches, as well as the GeoMod SA team (in particular **Gil Jacot-Descombes** and **Samuel Kivell**) for the supply of ZSoil models and the proofreading of this paper.

Table A.8
Complete list of random variables.

Variable	Formation	Parameter	
X0001	Fill	Friction angle	φ
X0002		Cohesion	c
X0003		Modulus	E_{oed}
X0004	Alluvium	Friction angle	φ
X0005		Cohesion	c
X0006		Modulus	E_{oed}
X0007	Upper limestones	Friction angle	φ
X0008		Cohesion	c
X0009		Modulus	E_{oed}
X0010	Medium limestones	Friction angle	φ
X0011		Cohesion	c
X0012		Modulus	E_{oed}
X0013	Lower limestones	Friction angle	φ
X0014		Cohesion	c
X0015		Modulus	E_{oed}
X0016	Upper clays	Friction angle	φ
X0017		Cohesion	c
X0018		Modulus	E_{oed}
X0019	Medium clays	Friction angle	φ
X0020		Cohesion	c
X0021		Modulus	E_{oed}
X0022	Lower clays	Friction angle	φ
X0023		Cohesion	c
X0024		Modulus	E_{oed}
X0025	MM limestones	Friction angle	φ
X0026		Cohesion	c
X0027		Modulus	E_{oed}
X0028	Chalk	Friction angle	φ
X0029		Cohesion	c
X0030		Modulus	E_{oed}
X0031	–	Confinement loss	λ
X0032	–	Water table height	h_w
X0033	–	Building load 1	F_1
X0034	–	Building load 2	F_2

Role of the funding source

This study has been financed by the “Ingénierie et Architecture” Domain of HES//SO, University of Applied Sciences Western Switzerland, which is acknowledged.

Appendix. Random variables

See Table A.8.

References

AFNOR, 2014. NF P94-500 - Geotechnical Engineering Missions - Classification and Specifications. French National Standard, Paris.

Al-Bittar, T., Soubra, A.-H., Thajeel, J., 2018. Kriging-based reliability analysis of strip footings resting on spatially varying soils. J. Geotech. Geoenviron. Eng. 144 (10), 04018071. http://dx.doi.org/10.1061/(ASCE)GT.1943-5606.0001958.

Ang, A.H.-S., Tang, W.H., 2007. Probability Concepts in Engineering: Emphasis on Applications in Civil & Environmental Engineering, second ed. Wiley, New York.

Baecher, G.B., Christian, J.T., 2003. Reliability and Statistics in Geotechnical Engineering. J. Wiley, Chichester, West Sussex, England.

CEN, 2002. EN 1990 – Basis of Structural Design. European Committee for Standardisation, Brussels.

CEN, 2004. EN 1997-1 – Geotechnical Design: General Rules. European Committee for Standardisation, Brussels.

Chen, F., Wang, L., Zhang, W., 2019. Reliability assessment on stability of tunnelling perpendicularly beneath an existing tunnel considering spatial variabilities of rock mass properties. Tunn. Undergr. Space Technol. 88, 276–289. http://dx.doi.org/10.1016/j.tust.2019.03.013.

Duncan, J.M., 2000. Factors of safety and reliability in geotechnical engineering. J. Geotech. Geoenviron. Eng. 126 (4), 307–316. http://dx.doi.org/10.1061/(ASCE)1090-0241(2000)126:4(307).

Echard, B., Gayton, N., Lemaire, M., 2011. AK-MCS: An active learning reliability method combining Kriging and Monte Carlo Simulation. Struct. Saf. 33 (2), 145–154. http://dx.doi.org/10.1016/j.strusafe.2011.01.002.

Fellin, W., Lessmann, H., Oberguggenberger, M., Vieider, R. (Eds.), 2005. Analyzing Uncertainty in Civil Engineering. Springer-Verlag, Berlin/Heidelberg, http://dx.doi.org/10.1007/b138177.

Fenton, G.A., Naghibi, F., Dundas, D., Bathurst, R.J., Griffiths, D., 2016. Reliability-based geotechnical design in 2014 Canadian Highway Bridge Design Code. Can. Geotech. J. 53 (2), 236–251. http://dx.doi.org/10.1139/cgj-2015-0158.

Gelman, A., Rubin, D.B., 1992. Inference from iterative simulation using multiple sequences. Statist. Sci. 7 (4), 457–472. http://dx.doi.org/10.1214/ss/1177011136.

Ghanem, R.G., Spanos, P.D., 1991. Stochastic Finite Elements: A Spectral Approach, Revised ed. Springer New York, New York, NY, http://dx.doi.org/10.1007/978-1-4612-3094-6.

Goodman, J., Weare, J., 2010. Ensemble samplers with affine invariance. Commun. Appl. Math. Comput. Sci. 5 (1), 65–80.

Gulvanessian, H., Calgaro, J.-A., Holický, M., Gulvanessian, H., 2012. In: Gulvanessian, H. (Ed.), Designers' Guide to Eurocode: Basis of Structural Design, second ed. ICE Publishing.

Guo, X., Dias, D., 2020. Kriging based reliability and sensitivity analysis – Application to the stability of an earth dam. Comput. Geotech. 120, 103411. http://dx.doi.org/10.1016/j.compgeo.2019.103411.

Hsiao, E.C., Schuster, M., Juang, C.H., Kung, G.T., 2008. Reliability analysis and updating of excavation-induced ground settlement for building serviceability assessment. J. Geotech. Geoenviron. Eng. 134 (10), 1448–1458. http://dx.doi.org/10.1061/(ASCE)1090-0241(2008)134:10(1448).

Huang, H., Su, W., Zhang, J., 2014. Selecting optimal probability models for geotechnical reliability analysis. In: International Conference of Geotechnical Safety and Risk IV. Taylor & Francis, London.

ISO 2394, 2015. ISO 2394:2015 - General Principles on Reliability for Structures. International Organization for Standardization.

JCSS, 2001. Probabilistic Model Code. Joint Committee on Structural Safety.

Kawa, M., Puła, W., Truty, A., 2021. Probabilistic analysis of the diaphragm wall using the hardening soil-small (HSs) model. Eng. Struct. 232, http://dx.doi.org/10.1016/j.engstruct.2021.111869.

Kayser, M., Gajan, S., 2014. Application of probabilistic methods to characterize soil variability and their effects on bearing capacity and settlement of shallow foundations: State of the art. Int. J. Geotech. Eng. 8, 352–364. http://dx.doi.org/10.1179/1938636213Z.00000000073.

Krige, D.G., 1951. A Statistical Approach to Some Mine Valuation and Allied Problems on the Witwatersrand (Master's thesis). University of the Witwatersrand, South Africa.

Kucherenko, S., Tarantola, S., Annoni, P., 2012. Estimation of global sensitivity indices for models with dependent variables. Comput. Phys. Comm. 183 (4), 937–946. http://dx.doi.org/10.1016/j.cpc.2011.12.020.

Lacasse, S., Nadim, F., 2007. Probabilistic geotechnical analyses for offshore facilities. Georisk: Assess. Manag. Risk Eng. Syst. Geohazards 1 (1), 21–42. http://dx.doi.org/10.1080/17499510701204224.

Leca, E., New, B., 2007. Settlements induced by tunneling in Soft Ground. Tunn. Undergr. Space Technol. 22 (2), 119–149. http://dx.doi.org/10.1016/j.tust.2006.11.001.

Lees, A., 2016. Geotechnical Finite Element Analysis: A Practical Guide. ICE Publishing.

Lemaire, M., 2009. Structural Reliability. ISTE and Wiley, London and Hoboken, NJ.

Li, Z., Gong, W., Li, T., Juang, C.H., Chen, J., Wang, L., 2021. Probabilistic back analysis for improved reliability of geotechnical predictions considering parameters uncertainty, model bias, and observation error. Tunn. Undergr. Space Technol. 115, 104051. http://dx.doi.org/10.1016/j.tust.2021.104051.

Low, B.K., 2017. Insights from reliability-based design to complement load and resistance factor design approach. J. Geotech. Geoenviron. Eng. 143 (11), 04017089. http://dx.doi.org/10.1061/(ASCE)GT.1943-5606.0001795.

Marelli, S., Lamas, C., Konakli, K., Mylonas, C., Wiederkehr, P., Sudret, B., 2021. UQLab User Manual – Sensitivity Analysis. Technical Report, Chair of Risk, Safety and Uncertainty Quantification, ETH Zurich, Switzerland.

Marelli, S., Sudret, B., 2014. UQLab: A framework for uncertainty quantification in Matlab. In: Vulnerability, Uncertainty, and Risk. American Society of Civil Engineers, Liverpool, UK, pp. 2554–2563. http://dx.doi.org/10.1061/9780784413609.257.

Marelli, S., Sudret, B., 2021. UQLab User Manual – Polynomial Chaos Expansions. Technical Report, Chair of Risk, Safety and Uncertainty Quantification, ETH Zurich, Switzerland.

Melchers, R.E., Beck, A.T., 2018. Structural Reliability Analysis and Prediction, third ed. Wiley, Hoboken, NJ.

Miro, S., Hartmann, D., Schanz, T., 2014. Global sensitivity analysis for subsoil parameter estimation in mechanized tunneling. Comput. Geotech. 56, 80–88. http://dx.doi.org/10.1016/j.compgeo.2013.11.003.

Obrzud, R., Truty, A., 2010. The Hardening Soil Model-A Practical Guidebook Z_Soil. Technical Report Z_Soil.PC100701, pp. 1–17.

Papaioannou, I., Betz, W., Straub, D., 2013. Bayesian model updating of a tunnel in soft soil with settlement measurements. https://citeseerx.ist.psu.edu/viewdoc/download;jsessionid=EAE05F7CEDFF6F979A643AFFA90662C6?doi=10.1.1.702.8255&rep=rep1&type=pdf.

Papaioannou, I., Straub, D., 2012. Reliability updating in geotechnical engineering including spatial variability of soil. Comput. Geotech. 42, 44–51. http://dx.doi.org/10.1016/j.compgeo.2011.12.004.

Phoon, K.-K., Ching, J. (Eds.), 2018. Risk and Reliability in Geotechnical Engineering. CRC Press, http://dx.doi.org/10.1201/b17970.

Phoon, K., Retief, J., 2015. ISO2394:2015 Annex d (Reliability of geotechnical structures). Georisk: Assess. Manag. Risk Eng. Syst. Geohazards 9 (3), 125–127. http://dx.doi.org/10.1080/17499518.2015.1077975.

Rocquigny, E.d., Devictor, N., Tarantola, S. (Eds.), 2008. Uncertainty in Industrial Practice: A Guide to Quantitative Uncertainty Management. J. Wiley, Chichester, England ; Hoboken, NJ.

Schöbi, R., Sudret, B., Marelli, S., 2017. Rare event estimation using polynomial-chaos kriging. ASCE-ASME J. Risk Uncertain. Eng. Syst. A 3 (2), D4016002. http://dx.doi.org/10.1061/AJRUA6.0000870.

Schöbi, R., Sudret, B., Wiart, J., 2015. Polynomial-Chaos-based Kriging. http://dx.doi.org/10.48550/ARXIV.1502.03939.

Sobol, I., 2001. Global sensitivity indices for nonlinear mathematical models and their Monte Carlo estimates. Math. Comput. Simulation 55 (1–3), 271–280. http://dx.doi.org/10.1016/S0378-4754(00)00270-6.

Straub, D., Papaioannou, I., 2015. Bayesian analysis for learning and updating geotechnical parameters and models with measurements. In: Risk and Reliability in Geotechnical Engineering. CRC Press, Taylor & Francis, http://dx.doi.org/10.1201/b17970.

Sudret, B., 2007. Uncertainty Propagation and Sensitivity Analysis in Mechanical Models–Contributions to Structural Reliability and Stochastic Spectral Methods (Habilitation a Diriger des Recherches). Université Blaise Pascal, Clermont-Ferrand, France.

Sudret, B., Commend, S., 2021. Uncertainty Quantification, Reliability and Sensitivity Analyses Applied to Geotechnics and Structures. Third Edition of Online Short Course.

Wagner, P.-R., Nagel, J., Marelli, S., Sudret, B., 2021. UQLab User Manual – Bayesian Inversion for Model Calibration and Validation. Technical Report, Chair of Risk, Safety and Uncertainty Quantification, ETH Zurich, Switzerland.

Wang, Y., Cao, Z., Li, D., 2016. Bayesian perspective on geotechnical variability and site characterization. Eng. Geol. 203, 117–125. http://dx.doi.org/10.1016/j.enggeo.2015.08.017.

Xiao, J., Luo, Z., Martin, J.R., Gong, W., Wang, L., 2016. Probabilistic geotechnical analysis of energy piles in granular soils. Eng. Geol. 209, 119–127. http://dx.doi.org/10.1016/j.enggeo.2016.05.006.

Zevgolis, I.E., Deliveris, A.V., Koukouzas, N.C., 2018. Probabilistic design optimization and simplified geotechnical risk analysis for large open pit excavations. Comput. Geotech. 103, 153–164. http://dx.doi.org/10.1016/j.compgeo.2018.07.024.

Zhang, Y., Commend, S., 2021. Calculs probabilistes des déplacements dus à la réalisation de tunnels à l'aide d'un modèle aux éléments finis. Rev. Fr. Géotech. 167 (5), http://dx.doi.org/10.1051/geotech/2021018.

Zhang, Y., Commend, S., Groslambert, M., 2022. Analyses et modélisations sur les argiles plastiques du Sparnacien du Bassin parisien. Rev. Fr. Géotech. 171 (3), http://dx.doi.org/10.1051/geotech/2022003.

Zhang, Y., Commend, S., Martin-Lavigne, Q., Lacoste, J., 2020b. The white house station of the grand Paris express project. Struct. Eng. Int. 30 (4), 460–467. http://dx.doi.org/10.1080/10168664.2019.1701966.

Zhang, W., Goh, A.T., 2012. Reliability assessment on ultimate and serviceability limit states and determination of critical factor of safety for underground rock caverns. Tunn. Undergr. Space Technol. 32, 221–230. http://dx.doi.org/10.1016/j.tust.2012.07.002.

Zhang, Y., Hamet, P., 2022. Estimation et Suivi des Déformations Induites par la Construction des Ouvrages et Tunnels, Vol. 281. Tunnels et Espace Souterrain, pp. 70–92.

Zhang, L.M., Ng, A.M.Y., 2005. Probabilistic limiting tolerable displacements for serviceability limit state design of foundations. Géotechnique 55 (2), 151–161. http://dx.doi.org/10.1680/geot.2005.55.2.151.

Zhang, Y., Toutlemonde, F., 2022. Calibrating partial safety factors in line with required reliability levels for concrete structures. Eur. J. Environ. Civ. Eng. 26 (9), 3863–3879. http://dx.doi.org/10.1080/19648189.2020.1824820.

Zhang, W., Zhang, R., Wu, C., Goh, A.T.C., Lacasse, S., Liu, Z., Liu, H., 2020a. State-of-the-art review of soft computing applications in underground excavations. Geosci. Front. 11 (4), 1095–1106. http://dx.doi.org/10.1016/j.gsf.2019.12.003.

Zhao, J., DeJong, M., 2023. Three-dimensional probabilistic assessment of tunneling induced structural damage using Monte-Carlo method and hybrid finite element model. Comput. Geotech. 154, 105122. http://dx.doi.org/10.1016/j.compgeo.2022.105122.

Zheng, H., Mooney, M., Gutierrez, M., 2023. Surrogate model for 3D ground and structural deformations in tunneling by the sequential excavation method. Comput. Geotech. 154, 105142. http://dx.doi.org/10.1016/j.compgeo.2022.105142.

ZSOIL.PC, 2020. A Windows-Based Tool offering a unified approach to numerical simulation of soil and rock mechanics, above & underground structures, excavations, soil-structure interaction and underground flow, including dynamics, thermal and moisture migration analysis. Version : v20.07.